



# An engineered 4-1BBL fusion protein with “activity on demand”

Jacqueline Mock<sup>a</sup>, Marco Stringhini<sup>a</sup>, Alessandra Villa<sup>b</sup>, Michael Weller<sup>c</sup>, Tobias Weiss<sup>c</sup>, and Dario Neri<sup>a,1</sup>

<sup>a</sup>Department of Chemistry and Applied Biosciences, Swiss Federal Institute of Technology (ETH Zürich), CH-8093 Zürich, Switzerland; <sup>b</sup>Antibody Research, Philochem AG, CH-8112 Otelfingen, Switzerland; and <sup>c</sup>Department of Neurology, University Hospital Zurich, University of Zurich, CH-8091 Zürich, Switzerland

Edited by Napoleone Ferrara, University of California San Diego, La Jolla, CA, and approved October 21, 2020 (received for review July 1, 2020)

**Engineered cytokines are gaining importance in cancer therapy, but these products are often limited by toxicity, especially at early time points after intravenous administration. 4-1BB is a member of the tumor necrosis factor receptor superfamily, which has been considered as a target for therapeutic strategies with agonistic antibodies or using its cognate cytokine ligand, 4-1BBL. Here we describe the engineering of an antibody fusion protein, termed F8-4-1BBL, that does not exhibit cytokine activity in solution but regains biological activity on antigen binding. F8-4-1BBL bound specifically to its cognate antigen, the alternatively spliced EDA domain of fibronectin, and selectively localized to tumors in vivo, as evidenced by quantitative biodistribution experiments. The product promoted a potent antitumor activity in various mouse models of cancer without apparent toxicity at the doses used. F8-4-1BBL represents a prototype for antibody-cytokine fusion proteins, which conditionally display “activity on demand” properties at the site of disease on antigen binding and reduce toxicity to normal tissues.**

armed antibody | protein engineering | tumor targeting | 4-1BB | cancer immunotherapy

Cytokines are immunomodulatory proteins that have been considered for pharmaceutical applications in the treatment of cancer patients (1–3) and other types of disease (2). There is a growing interest in the use of engineered cytokine products as anticancer drugs, capable of boosting the action of T cells and natural killer (NK) cells against tumors (3, 4), alone or in combination with immune checkpoint inhibitors (3, 5–7).

Recombinant cytokine products on the market include interleukin-2 (IL-2) (Proleukin) (8, 9), IL-11 (Neumega) (10, 11), tumor necrosis factor (TNF; Beromun) (12), interferon (IFN)- $\alpha$  (Roferon A, Intron A) (13, 14), IFN- $\beta$  (Avonex, Rebif, Betaseron) (15, 16), IFN- $\gamma$  (Actimmune) (17), granulocyte colony-stimulating factor (Neupogen) (18), and granulocyte macrophage colony-stimulating factor (Leukine) (19, 20). The recommended dose is typically very low (often <1 mg/d) (21–23), as cytokines may exert biological activity in the subnanomolar concentration range (24). Various strategies have been proposed to develop cytokine products with improved therapeutic index. Protein PEGylation or Fc fusions may lead to prolonged circulation time in the bloodstream, allowing the administration of low doses of active payload (25, 26). In some implementations, cleavable polyethylene glycol polymers may be considered, yielding prodrugs that regain activity at later time points (27). Alternatively, tumor-homing antibody fusions have been developed, since the preferential concentration of cytokine payloads at the tumor site has been shown in preclinical models to potentiate therapeutic activity, helping spare normal tissues (28–34). Various antibody-cytokine fusions are currently being investigated in clinical trials for the treatment of cancer and of chronic inflammatory conditions (reviewed in refs. 2, 33, 35–37).

Antibody-cytokine fusions display biological activity immediately after injection into patients, which may lead to unwanted toxicity and prevent escalation to therapeutically active dosage regimens (9, 22, 38). In the case of proinflammatory payloads

(e.g., IL-2, IL-12, TNF- $\alpha$ ), common side effects include hypotension, nausea, and vomiting, as well as flu-like symptoms (24, 39–42). These side effects typically disappear when the cytokine concentration drops below a critical threshold, thus providing a rationale for slow-infusion administration procedures (43). It would be highly desirable to generate antibody-cytokine fusion proteins with excellent tumor-targeting properties and with “activity on demand”—biological activity that is conditionally gained on antigen binding at the site of disease, helping spare normal tissues.

Here we describe a fusion protein consisting of the F8 antibody specific to the alternatively spliced extra domain A (EDA) of fibronectin (44, 45) and of murine 4-1BBL, which did not exhibit cytokine activity in solution but could regain potent biological activity on antigen binding. The antigen (EDA+ fibronectin) is conserved from mouse to man (46), is virtually undetectable in normal adult tissues (with the exception of the placenta, endometrium, and some vessels in the ovaries), but is expressed in the majority of human malignancies (44, 45, 47, 48). 4-1BBL, a member of the TNF superfamily (49), is expressed on antigen-presenting cells (50, 51) and binds to its receptor, 4-1BB, which is up-regulated on activated cytotoxic T cells (52), activated dendritic cells (52), activated NK and NKT cells (53), and regulatory T cells (54). Signaling through 4-1BB on cytotoxic T cells protects them from activation-induced cell death and skews the cells toward a more memory-like phenotype (55, 56).

## Significance

**Antibody-cytokine fusion proteins have been successfully applied for the treatment of preclinical models of cancer and have yielded promising results in early clinical trials. The antibody moiety redirects the immunostimulatory payload to the tumor to boost the antitumor immune response. However, especially at early time points after administration, the relatively high concentration of the antibody-cytokine conjugate in blood can lead to severe side effects due to peripheral activation of cytokine receptors. Therefore, protein engineering approaches are needed to develop antibody-cytokine conjugates that selectively regain their immunostimulatory activity on antigen binding in the tumor. In this work, we have developed an antibody-cytokine conjugate that meets these criteria and shows antitumor activity in preclinical models of cancer.**

Author contributions: J.M., M.S., M.W., and D.N. designed research; J.M., M.S., and T.W. performed research; J.M., A.V., and T.W. contributed new reagents/analytic tools; J.M., M.S., and T.W. analyzed data; J.M. and D.N. wrote the paper; and M.W. coordinated the study in glioblastoma.

Competing interest statement: D.N. is a cofounder and shareholder of Philogen S.p.A., the company that owns the F8 and L19 antibodies.

This article is a PNAS Direct Submission.

Published under the PNAS license.

<sup>1</sup>To whom correspondence may be addressed. Email: dario.neri@pharma.ethz.ch.

This article contains supporting information online at <https://www.pnas.org/lookup/suppl/doi:10.1073/pnas.2013615117/-DCSupplemental>.

First published November 25, 2020.

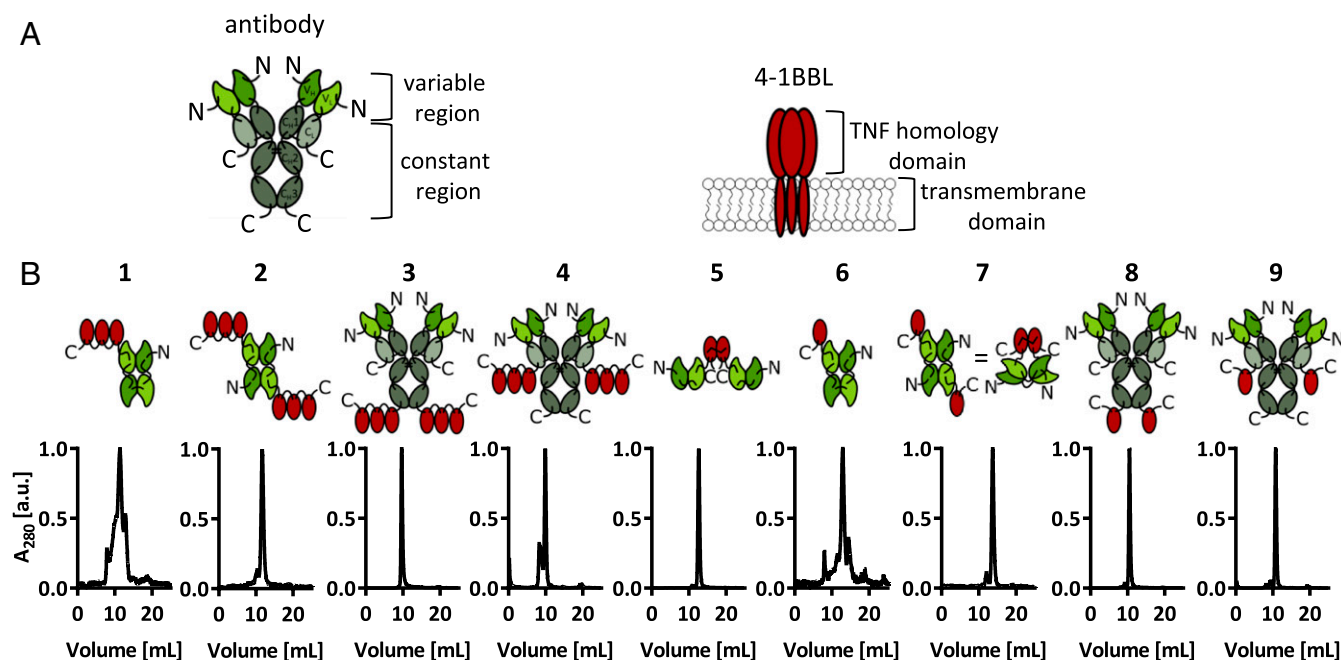


**Fig. 1.** The nine F8-4-1BBL fusion proteins designed and tested in this study. (A) schematic depiction of an antibody in the IgG format and of human 4-1BBL, a transmembrane protein which forms a noncovalent homotrimer (57). (B) Schematic depiction of the fusion proteins featuring murine 4-1BBL and size exclusion chromatograms.

We engineered nine formats of the F8-4-1BBL fusion protein, one of which exhibited superior performance in quantitative biodistribution studies and conditional gain of cytokine activity on antigen binding. The antigen-dependent reconstitution of the biological activity of the immunostimulatory payload represents an example of an antibody fusion protein with “activity on demand.” The fusion protein was potentially active against different types of cancer without apparent toxicity at the doses used. The EDA of fibronectin is a particularly attractive antigen for cancer therapy in view of its high selectivity, stability, and abundant expression in most tumor types (44, 45, 47, 48).

## Results

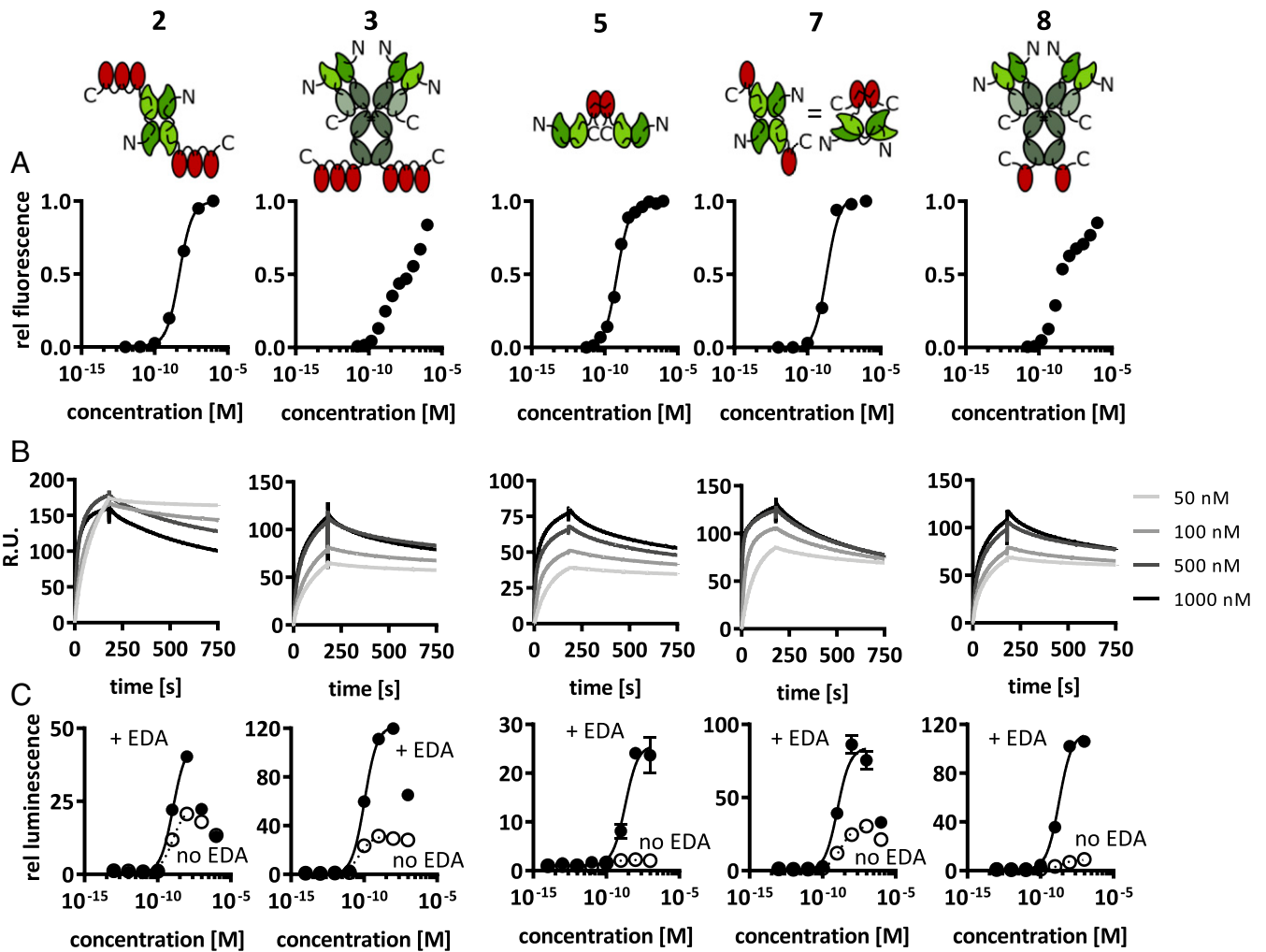
Human 4-1BBL is a homotrimeric protein (Fig. 1A) (57), while its murine counterpart forms stable homodimers (58, 59). Stable trimeric structures can be engineered by connecting 4-1BBL monomeric domains with suitable polypeptide linkers (60). Recombinant antibodies can be expressed as full IgG or as fragments, forming single-chain Fv (scFv) (61, 62) or diabody (63) structures (Fig. 1B and *SI Appendix, Table S1*) (2, 64, 65). To identify products with promising features for subsequent *in vivo* investigations, nine different fusion proteins containing F8 antibody and murine 4-1BBL moieties were expressed in mammalian cells. Mutational scans had revealed that the disulfide bond linking two 4-1BBL monomers is crucial for protein stability (*SI Appendix, Fig. S1*). The observation that the TNF homology domain (THD) within 4-1BBL was sufficient for full *in vitro* activity (*SI Appendix, Fig. S2*) guided the design of the modules to be included in the fusion proteins. Six of the nine products exhibited favorable size exclusion and SDS/PAGE profiles (Fig. 1B and *SI Appendix, Fig. S3*). We selected formats 2, 3, 5, 7, and 8 for further investigations, since those proteins gave the best yields and did not show signs of aggregation even after repeated freeze-thaw cycles.

Fig. 2 presents a comparative analysis of *in vitro* properties of F8-4-1BBL in various formats. The 4-1BBL and F8 moieties were able to recognize the cognate targets in the 2, 3, 5, 7, and 8 formats. Indeed, all proteins bound with high affinity to murine CTLL-2 cells, which are strongly positive for murine 4-1BB (the

4-1BBL receptor) (Fig. 2A) and to recombinant EDA of fibronectin (Fig. 2B). A functional assay with a nuclear factor kappa light-chain enhancer of activated B cells (NF- $\kappa$ B) reporter cell line (66) revealed that all fusion proteins preferentially activated downstream signaling events in the presence of the cognate fibronectin EDA antigen, immobilized on a solid support and thus mimicking the tumor environment (Fig. 2C). Formats 5 [consisting of two disulfide-linked 4-1BBL monomeric units fused to scFv(F8)] and 8 [in which monomeric units of 4-1BBL were fused at the C-terminal ends of the heavy chains of IgG(F8)] exhibited the best discrimination between low biological activity in solution and high cytokine activity in the presence of antigen. For this reason, formats 5 and 8 were selected for an *in vivo* characterization of their tumor-targeting properties. Format 2 was also included in the comparison, since diabody-based antibody cytokine fusion proteins have previously been used for clinical development programs (2, 64).

Protein preparations were radioiodinated and injected into immunocompetent 129/Sv mice bearing subcutaneously (s.c.) grafted murine F9 teratocarcinomas, which express EDA of fibronectin around tumor blood vessels (44). Mice were euthanized at 24 h after intravenous (i.v.) administration, and biodistribution results were expressed as percentage of injected dose per gram of tissue (%ID/g) (Fig. 3A and *SI Appendix, Fig. S4*). Format 2 exhibited only a modest tumor uptake (1.0% ID/g) and poor selectivity. Format 8 showed, as expected, a longer circulatory half-life, as evidenced by the high %ID/g in blood after 24 h, but the tumor uptake and selectivity were not significantly higher compared with KSF-4-1BBL (a fusion protein based on the KSF antibody, specific to hen egg lysozyme and serving as negative control) (67). By contrast, format 5 exhibited a preferential accumulation in the tumor (2.8% ID/g) and a good tumor-to-normal organ selectivity. EDA targeting was essential for tumor homing, as revealed by the comparison of the biodistribution results with the negative control KSF-4-1BBL fusion protein (Fig. 3A and *SI Appendix, Fig. S4*).

To confirm selective tumor uptake with a different methodology, format 5 was injected into tumor-bearing mice. An *ex vivo*



**Fig. 2.** In vitro characterization of five F8-4-1BBL formats. (A) Binding to 4-1BB was measured by flow cytometry with the murine cytotoxic T cell line CTLL-2, which expresses 4-1BB. (B) Binding of the F8 moiety to the EDA-positive ectodomain of fibronectin was measured by surface plasmon resonance on chips coated with recombinant EDA. (C) Biological activity was tested using an NF- $\kappa$ B reporter cell line that secretes luciferase on activation of the NF- $\kappa$ B pathway by signaling through 4-1BB. The assay was performed both with and without EDA immobilized on solid support ( $n = 3$ ). Curve fitting was done using the agonist vs. response (three-parameter) fit of GraphPad Prism 7.0. Data represent mean  $\pm$  SD.

immunofluorescence analysis revealed a preferential accumulation of format 5 around tumor blood vessels, while no staining was detectable in normal organs or when the KSF fusion protein was used (Fig. 3B and *SI Appendix, Fig. S5*). In line with previous reports on this matter (44, 45, 47, 48), the EDA of fibronectin is an ideal target for pharmacodelivery applications in mouse and human, as the antigen is undetectable in normal adult tissues but is strongly expressed in the stroma and around the blood vessels in many different tumor types (*SI Appendix, Fig. S6*).

Therapeutic studies were performed using format 5 of F8-4-1BBL, both in a preventive setting starting at a tumor volume of 40 mm<sup>3</sup> and in a therapeutic setting starting at a tumor volume of 75 to 100 mm<sup>3</sup>. In a preventive setting in WEHI-164 fibrosarcomas, three out of five mice rejected the tumor using F8-4-1BBL as single-agent therapy, while four out of five mice showed a complete response when treated with PD-1 blockade either alone or in combination with F8-4-1BBL (Fig. 4A). The cured mice rejected subsequent challenges with WEHI-164 fibrosarcoma cells. In some cured mice, a challenge with CT26 colon carcinoma cells was also rejected, similar to what we had previously reported for other F8-based immunocytokine therapeutics (68, 69) (*SI Appendix, Fig. S7*). When the therapy was repeated

in mice bearing larger WEHI-164 fibrosarcoma tumors, significant tumor growth retardation was observed in mice treated with F8-4-1BBL ( $P = 0.0427$ , regular two-way ANOVA with Tukey's multiple comparison test; day 13) (Fig. 4B). There was no difference in tumor growth between mice receiving injections of saline and those receiving the KSF fusion proteins, underscoring the importance of the antigen-dependent activation of 4-1BBL (Fig. 4B). Similar experiments performed in immunocompetent mice bearing CT26 tumors showed a tumor regression in four of five mice treated with F8-4-1BBL. One mouse was cured, while tumors eventually regrew in the other mice. Therapy was also potent when F8-4-1BBL was combined with PD-1 blockade (Fig. 4C).

All treatments in all experiments were well tolerated, as indicated by the absence of body weight loss (Fig. 4). When MC38 colon carcinoma-bearing mice were treated with F8-4-1BBL or PD-1 blockade as single agents, moderate tumor growth retardation was observed compared with mice treated with saline ( $P < 0.0001$ , regular two-way ANOVA with Tukey's multiple comparison test; day 12). By contrast, the combination treatment was potently active and led to durable complete remissions in two of six mice (Fig. 4D).

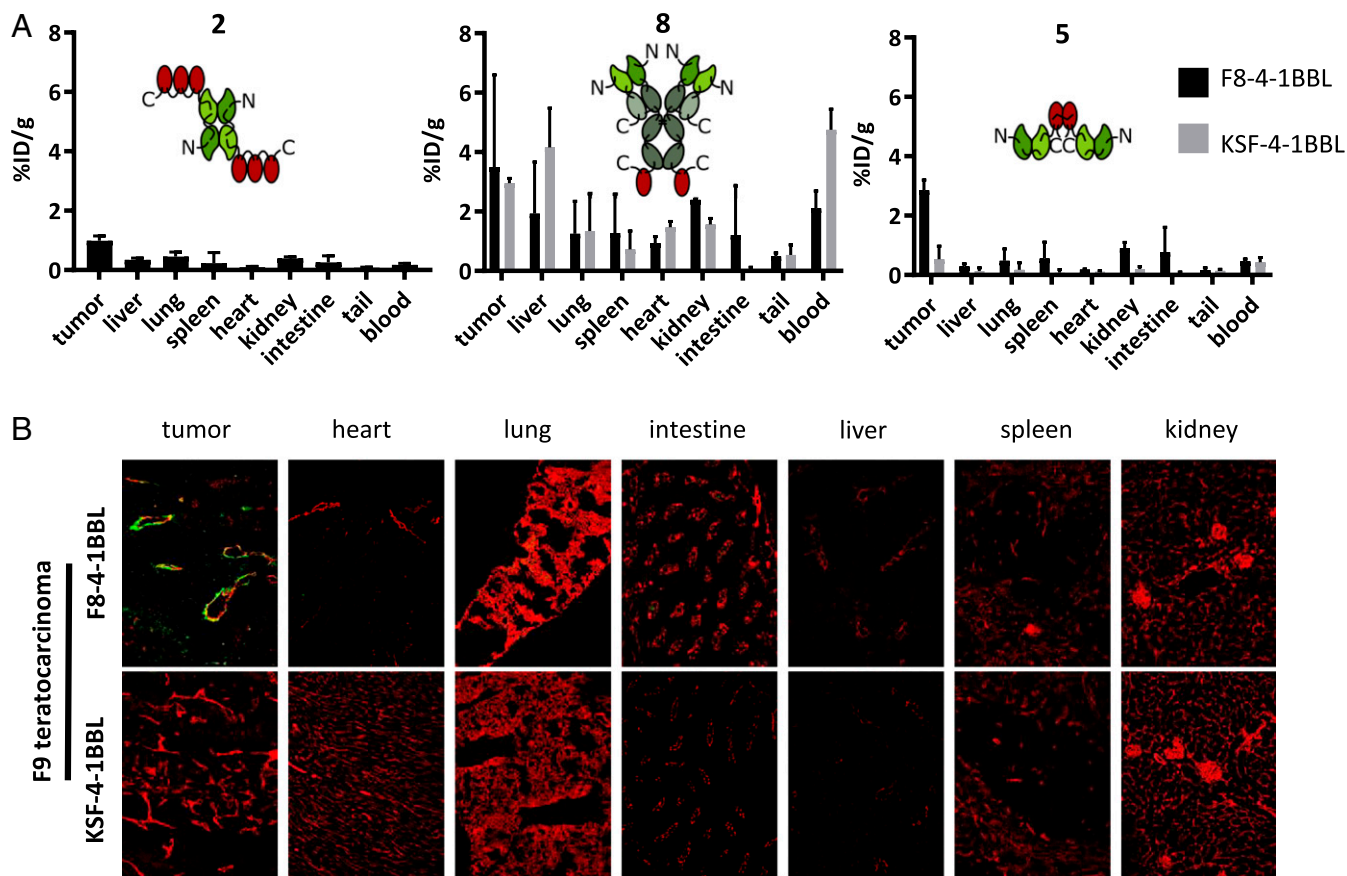


**Fig. 3.** In vivo biodistribution studies of three F8-4-1BBL formats. (A) The mice were euthanized at 24 h after injection of the radioiodinated proteins, and the radioactivity of excised organs was measured and expressed as percent injected dose per gram of tissue ( $\%ID/g \pm SD$ ,  $n = 3$ ). The KSF antibody targeting hen egg lysozyme served as an untargeted control (67). (B) The mice were euthanized at 24 h after the injection of FITC-labeled F8-4-1-BBL or KSF-4-1-BBL in format 5. The proteins were detected ex vivo on cryosections (green,  $\alpha$ FITC; red,  $\alpha$ CD31).

To further investigate the therapeutic activity of F8-4-1BBL alone and in combination with PD-1 blockade, we studied an orthotopic model of glioblastoma in immunocompetent mice. Treatment was started 5 d after intracerebral implantation of GL-261 tumor cells. Mice were imaged at day 12 by magnetic resonance imaging (MRI) and were monitored in terms of body weight and behavior, then euthanized when they developed neurologic symptoms. In keeping with previous reports, none of the mice from the saline treatment group survived more than 20 d. By contrast, F8-4-1BBL exhibited potent anticancer activity, which was potentiated by PD-1 blockade. Eighty percent of the mice in the combination treatment group were rendered tumor-free, as evidenced by both MRI analysis and survival data (Fig. 4E).

To analyze the tumor-infiltrating leukocytes, mice were euthanized at 48 h after the second cycle of injections. Tumors and tumor-draining lymph nodes were excised, homogenized, and stained for analysis by flow cytometry. CT26 tumors were found to be highly infiltrated by lymphocytes, in keeping with previous reports (70–72), while WEHI-164 lesions were immunologically rather “cold” (Fig. 5A). The proportion of  $CD8^+$  T cells specific to AH1, a retroviral antigen that has a dominant role in the rejection of tumors implanted in BALB/c mice (69, 73), was higher in CT26 tumors (Fig. 5A). Treatment with F8-4-1BBL led to a significant increase in intratumoral  $CD3^+$  T cell density in both models, but the proportion of  $CD4^+$  or  $CD8^+$  T cells did not vary substantially. No difference was observed in terms of regulatory T cell (Treg) density (Fig. 5A). In keeping with previous reports (74), the proportion of AH1-specific  $CD8^+$  T cells

did not vary substantially as a result of pharmacologic treatment (Fig. 5A). Treatment with F8-4-1BBL led to decreases in  $CD3^+$  and  $CD4^+$  T cells in the tumor-draining lymph nodes, with a concomitant increase in antigen-presenting cells in CT26 tumor-bearing mice (but not in WEHI-164) (Fig. 5B). An increase in the proportion of effector T cells ( $CD44^+CD62L^-$ ) was observed among the AH1-specific  $CD8^+$  T cells in the tumor-draining lymph nodes (Fig. 5C). Virtually all tumor-infiltrating  $CD8^+$  T cells were positive for the exhaustion markers PD-1 and CD39 (Fig. 5C) (75, 76). The gating strategy used in the study is shown in *SI Appendix, Fig. S8*. Collectively, the markers used in this study did not detect a phenotypic change in tumor-infiltrating T cells, but an increase in effector T cells was observed for the AH1-specific  $CD8^+$  T cell population in tumor-draining lymph nodes as a result of F8-4-1BBL treatment.

## Discussion

We have described the development of an antibody-cytokine fusion protein targeted to the tumor neovasculature, featuring an engineered murine homodimeric 4-1BBL moiety as an immunostimulatory payload. Some formats were completely inactive in solution, while others retained low biological activity in the absence of antigen. The low constitutive biological activity of the formats featuring two single-chain trimeric ligands could be due to a residual receptor clustering triggered by hexameric 4-1BBL. The size exclusion profile of format 7 revealed the presence of a minor fraction of aggregated protein, which could potentially trigger some downstream signaling; however, since it

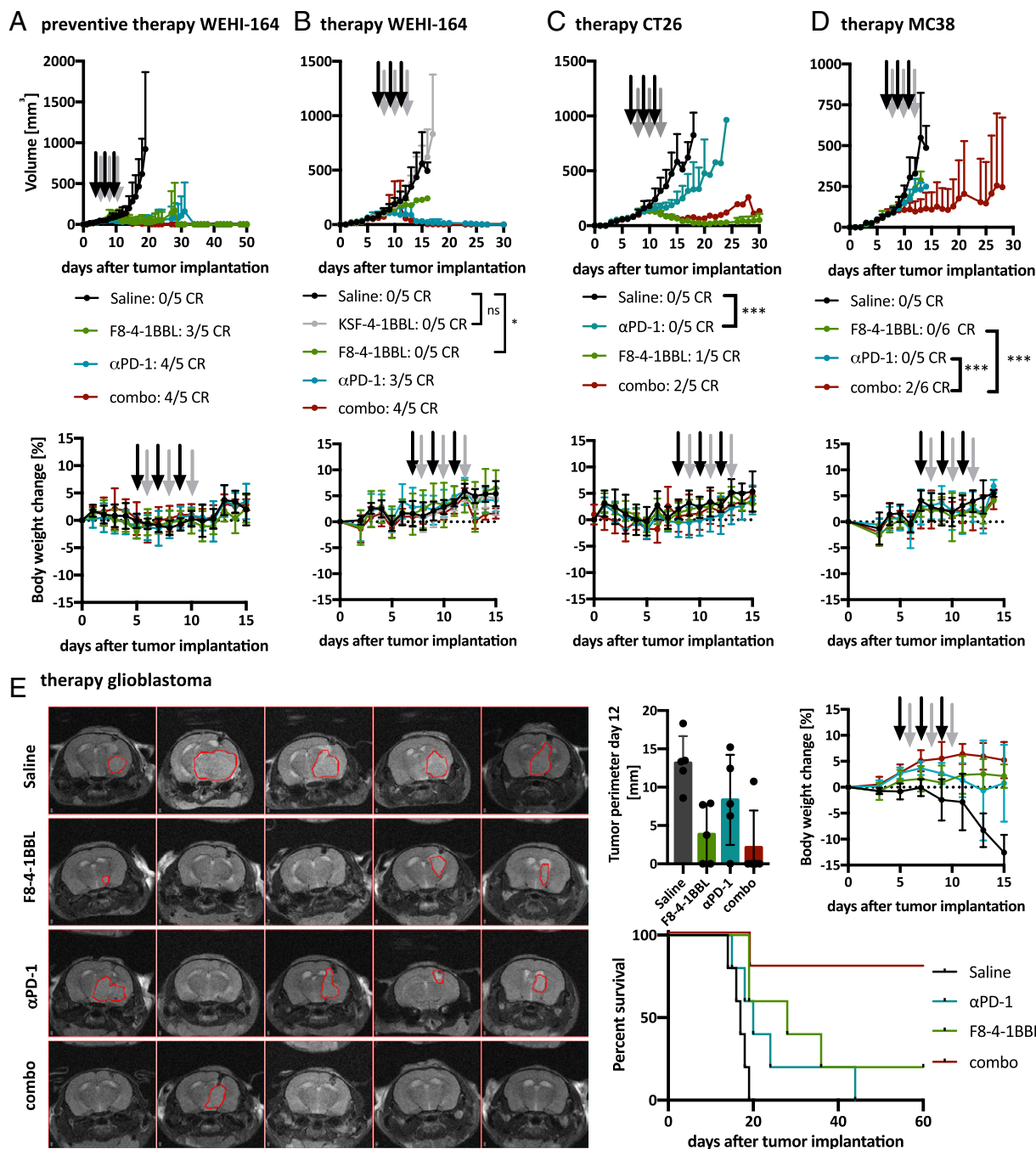


**Fig. 4.** Therapy studies with F8-4-1BBL in format 5. (A) Preventive therapy in WEHI-164 fibrosarcoma-bearing mice was started on day 5 when the tumors reached a volume of 40 mm<sup>3</sup>. The tumor sizes are shown as mean + SD (*n* = 5). The body weight data are represented as mean body weight change ± SD for each group. (B) Therapy in WEHI-164 fibrosarcoma-bearing mice was started on day 7 when the tumor volume was >80 mm<sup>3</sup>. The tumor sizes are shown as mean + SD (*n* = 5). The statistical results of regular two-way ANOVA followed by Tukey's multiple comparison test using GraphPad Prism 8.4.1 on day 13 are shown. ns, not significant; \**P* = 0.0427. The body weight data are represented as mean body weight change ± SD for each group. (C) In CT26-colon carcinoma-bearing mice, therapy was started on day 7 when the tumor volume exceeded 80 mm<sup>3</sup>. The tumor sizes are shown as mean + SD (*n* = 5). The result of a regular two-way ANOVA followed by Tukey's multiple comparison test using GraphPad Prism 8.4.1 revealed that as of day 13, the tumor size was significantly smaller in the mice treated with PD-1 blockade compared with the mice treated with saline (\*\**P* = 0.0004). The body weight data are represented as mean body weight change ± SD for each group. (D) In MC-38 colon carcinoma-bearing mice, therapy was started on day 7 when the tumor volume exceeded 75 mm<sup>3</sup>. The tumor sizes are shown as mean + SD (*n* = 5 or 6). The result of a regular two-way ANOVA followed by a Tukey's multiple comparison test using GraphPad Prism 8.4.1 is shown for day 12 (\*\**P* < 0.001). The body weight data are represented as mean body weight change ± SD for each group. (E) GL-261 was implanted orthotopically in C57BL/6 mice. Subsequently, mice were treated i.v. with saline, F8-4-1BBL, αPD-1, or the combination starting on day 5. Tumor size was assessed at day 12 after tumor implantation. (Left) MRI with tumors outlined in red. (Right) Quantification of tumor perimeters (*n* = 5). The survival data are presented as Kaplan–Meier plots (*n* = 5). Results from a Gehan–Breslow–Wilcoxon test reveal significant (*P* = 0.0036) differences between the survival curves of the different treatment groups. The body weight data are represented as mean body weight change ± SD for each group. Black arrows denote injections of the single agents, and gray arrows denote injection of F8-4-1BBL in the combination treatment. CR, complete response.

was not possible to remove the aggregated fraction, this hypothesis could not be experimentally proven. Subtle variations in the molecular format were observed not only to lead to different performance *in vitro*, but also to affect the biodistribution properties *in vivo*. Both preferential localization in the tumor and antigen-dependent gain in activity are prerequisites for restricting the activity of the fusion protein to the site of disease. The selected format **5** was inactive in solution but regained activity on clustering on the antigen. Favorable tumor-targeting results and potent tumor growth inhibition were observed *in vivo*, making F8-4-1BBL a promising prototype for the development of next-generation immunocytokines with antigen-dependent activation properties.

4-1BB, the receptor for 4-1BBL, has been recognized as an important target for cancer immunotherapy, as this member of the TNF receptor superfamily delivers costimulatory signals to activated cytotoxic T cells (77). The first 4-1BB agonistic antibody, urelumab, showed promising anticancer activity in preclinical models, but unfortunately demonstrated substantial hepatotoxicity in clinical trials (78). The hepatic toxicity was due mainly to the activation of liver Kupffer cells and monocytes, leading to a massive infiltration by T cells (78, 79).

Efforts are underway to develop 4-1BB agonists with more favorable toxicity profiles that retain potent costimulatory capacities (80–82). In addition to the optimization of anti-4-1BB immunoglobulins (80, 81), various formats of targeted 4-1BB agonists are being investigated. Bispecific antibodies capable of simultaneous recognition of 4-1BB and of tumor-associated antigens (e.g., EGFR, CEA) have been developed and tested in preclinical models of cancer with encouraging results (82, 83). Novel formats of targeted 4-1BB agonists have recently been considered for clinical development. An FAP-targeted immunocytokine with trimeric single-chain 4-1BBL has recently started phase I clinical testing in cancer patients (84). A fusion protein of trastuzumab with a 4-1BB-specific anticalin has shown antigen-dependent modulation of 4-1BB agonistic activity *in vitro* and has recently started clinical trials (85).

The search for antibody-cytokine products with “activity on demand” has been recognized as an important research goal to generate products with improved activity and safety profiles (86, 87). One possible strategy features the use of cytokine-binding polypeptides acting as proteolytically cleavable inhibitory moieties (88). Fusing cytokines at the C-terminal end of the IgG light chain may restrict conformational changes in the hinge region and slightly modulate cytokine activity on antibody binding to the cognate antigen (87). The attenuation of cytokine potency by targeted mutagenesis has been considered as a strategy to increase the dose of antibody-cytokine fusion proteins (89) or to conditionally activate tumor cells that express both a tumor-associated antigen and a cytokine receptor (e.g., IFN- $\alpha$  receptor) on their surface (90, 91). In addition, the targeted reconstitution of antibodies fused with “split-cytokine” moieties (i.e., subunits of heterodimeric cytokines that can reassemble at the tumor site) has been reported. Until now, the performance of that approach has been limited by the fact that the cytokine subunits used in the study (e.g., the p35 chain of IL12) retained biological activity (92).

Most ligands of the TNF superfamily, including human 4-1BBL, form homotrimers instead of homodimers, as is the case for murine 4-1BBL (93). However, activation of receptors of the TNF superfamily requires higher-order multimerization. The approach described in this article may be generally applicable to members of the TNF superfamily (60) if stable homodimers can be generated as payloads for antibody fusion. Alternative approaches may involve bispecific antibodies (94, 95) or the modular use of small protein domains (85, 96) or chemically modified bicyclic peptides (97). Members of the TNF receptor superfamily are particularly suited for cooperative activation strategies in view of their homotrimeric structure and clustering-driven

activation properties (98–100). The development of immunotherapeutics with “activity on demand” for monomeric cytokines may be more challenging, as protein assembly cannot be relied on for the reconstitution of biological activity.

## Materials and Methods

**Cell Lines.** The murine cytotoxic T cell line CTLL-2 (ATCC TIB-214), murine F9 teratocarcinoma cell line (ATCC CRL-1720), murine WEHI-164 fibrosarcoma cell line (ATCC CRL-1751), and murine CT26 colon carcinoma cell line (ATCC CRL-2638) were obtained from ATCC. The MC38 colon carcinoma cell line was a kind gift from Onur Boyman, Department of Immunology, University Hospital Zurich, Zurich, Switzerland. The cells were expanded and stored as cryopreserved aliquots in liquid nitrogen. The CTLL-2 cells were grown in RPMI 1640 (Gibco, 21875034) supplemented with 10% FBS (Gibco, 10270106), 1 $\times$  antibiotic-antimycoticum (Gibco, 15240062), 2 mM ultraglutamine (Lonza, BE17-605E/U1), 25 mM Hepes (Gibco, 15630080), 50  $\mu$ M  $\beta$ -mercaptoethanol (Sigma-Aldrich), and 60 U/mL human IL-2 (Proleukin; Roche Diagnostics). The F9 teratocarcinoma cells were grown in DMEM (Gibco; high glucose, pyruvate, 41966-029) supplemented with 10% FBS (Gibco, 10270106) and 1 $\times$  antibiotic-antimycoticum (Gibco, 15240062) in flasks coated with 0.1% gelatin (type B from bovine skin; Sigma-Aldrich, G1393). The WEHI-164 fibrosarcoma and the CT26 colon carcinoma were grown in RPMI 1640 (Gibco, 21875034) supplemented with 10% FBS (Gibco, 10270106) and 1 $\times$  antibiotic-antimycoticum (Gibco, 15240062). The MC38 colon carcinoma cells were grown in Advanced DMEM (Gibco, 12491915) supplemented with 10% FBS (Gibco, 10270106), 1 $\times$  antibiotic-antimycoticum (Gibco, 15240062), and 2 mM ultraglutamine (Lonza, BE17-605E/U1). GL-261 cells were obtained from the National Cancer Institute and cultured as described previously (101, 102). The cells were passaged at the recommended ratios and never kept in culture for longer than 1 mo.

**Mice.** Eight-wk-old female C57BL/6, BALB/c, and 129/Sv mice were obtained from Janvier. After at least 1 wk of acclimatization, 10<sup>7</sup> F9 cells, 2.5  $\times$  10<sup>6</sup> WEHI-164 cells, and 4  $\times$  10<sup>6</sup> CT26 or 10<sup>6</sup> MC38 cells were s.c. implanted into the right flank. Tumor size was monitored daily by caliper measurements, and the volume was calculated using the formula [length  $\times$  width  $\times$  width  $\times$  0.5]. For studies in mouse models of glioblastoma, 8-wk-old female C57BL/6 mice were purchased from Charles River Laboratories. Intracranial tumor cell implantation has been described previously (101). The animal experiments were carried out under project licenses ZH04/2018 (s.c. tumor models) and ZH73/2018 (glioblastoma) granted by the Veterinäramt des Kantons Zürich, in compliance with the Swiss Animal Protection Act (TSchG) and the Swiss Animal Protection Ordinance (TSchV).

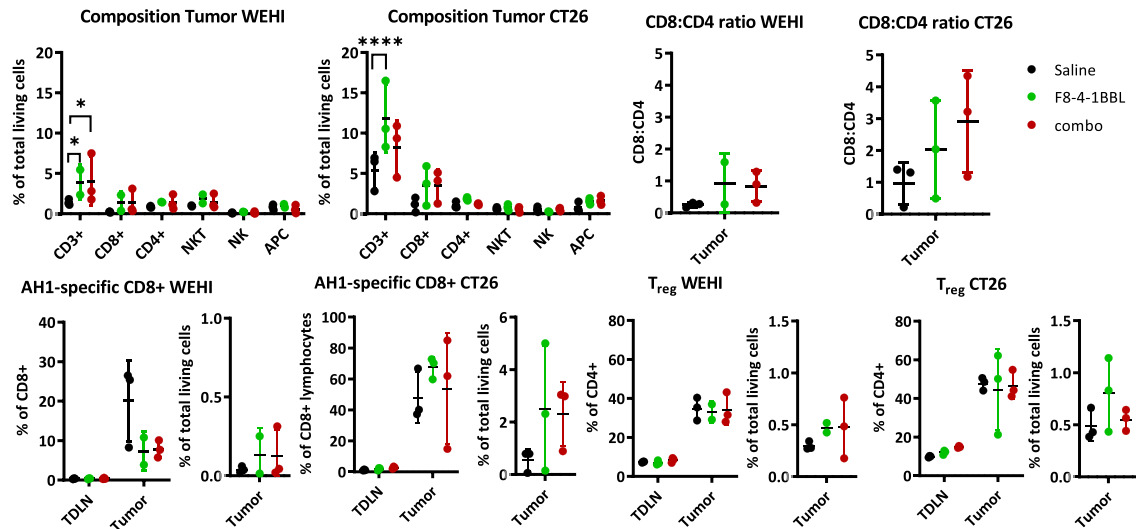
**Cloning.** The genetic constructs were created by standard cloning methods. The details are provided in *SI Appendix*.

**Protein Production.** Proteins were produced by transient transfection of CHO-S cells and purified by protein A affinity chromatography as described previously (68, 103, 104). Quality control of the purified products included SDS/PAGE and size exclusion chromatography using the Äkta Pure fast protein liquid chromatography system (GE Healthcare) with a Superdex S200 10/300 increase column at a flow rate of 0.75 mL/min (GE Healthcare) (Fig. 1 and *SI Appendix*, Fig. S1).

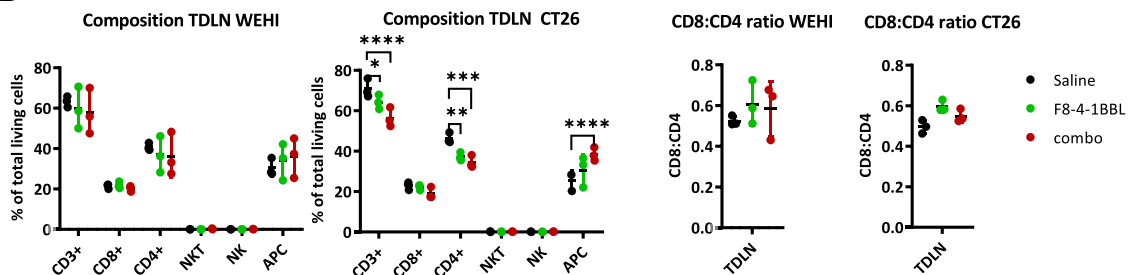
**Binding Measurements by Surface Plasmon Resonance.** To evaluate the binding kinetics of the F8 antibody fragment to EDA, a CM5 sensor chip (GE Healthcare) was coated with approximately 500 resonance units of an EDA-containing recombinant fragment of fibronectin. The measurements were carried out with a Biacore S200 analysis system (GE Healthcare). The contact time was set to 3 min at a flow rate of 20  $\mu$ L/min, followed by dissociation for 10 min and regeneration of the chip using 10 mM HCl.

**Binding Measurements by Flow Cytometry.** To measure the binding of the 4-1BBL moiety to cells expressing 4-1BB, CTLL-2 cells were incubated with varying concentrations of the fusion proteins for 1 h. The bound protein was detected by addition of an excess of Alexa Fluor 488-labeled protein A (Thermo Fisher Scientific, P11047) and subsequent measurement of fluorescence using a CytoFLEX flow cytometer (Beckman Coulter). The mean fluorescence was normalized, and the resulting binding curve was fitted using the agonist vs. response three-parameter fit of GraphPad Prism 7.0 to estimate the functional  $K_D$  value.

### A TILs in WEHI-164 fibrosarcoma and CT26 colon carcinoma



### B composition of the tumor-draining lymph nodes (TDLNs)



### C phenotype of TILs in CT26

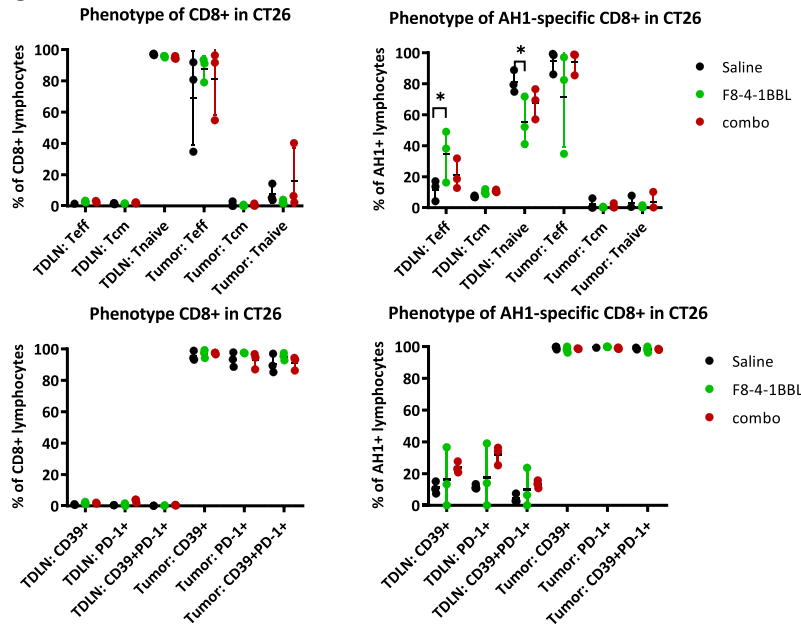


**Fig. 5.** Analysis of tumor-infiltrating leukocytes (TILs) and tumor-draining lymph nodes (TDLNs). (A) Composition of the tumor-infiltrating immune cells, including the CD8:CD4 ratio, the proportions of AH1-specific CD8<sup>+</sup> T cells and regulatory CD4<sup>+</sup> T cells in WEHI-164 and CT26 tumors treated with saline, F8-4-1BBL, and combination therapy ( $\alpha$ PD-1 and F8-4-1BBL). The proportions of AH1-specific CD8<sup>+</sup> T cells and regulatory CD4<sup>+</sup> T cells are shown also for matching TDLNs. (B) Composition of the TDLNs in WEHI-164 and CT26 tumor-bearing mice, including the CD8:CD4 ratio. (C) Phenotype of the CD8<sup>+</sup> T cells and AH1-specific CD8<sup>+</sup> T cells in CD26 tumor-bearing mice from different treatment groups. The phenotype was assessed based on the expression of CD62L, CD44, and the exhaustion markers CD39 and PD-1. The data represent individual values, means, and SDs. Statistical evaluations were performed using a regular two-way ANOVA followed by Tukey's multiple comparison test using GraphPad Prism 8.4.1. \* $P < 0.05$ ; \*\* $P < 0.01$ ; \*\*\* $P < 0.001$ ; \*\*\*\* $P < 0.0001$ . APC, antigen-presenting cell; Treg, regulatory T cell; Teff, effector T cell (CD44<sup>+</sup>CD62L<sup>+</sup>); Tcm, central memory T cell (CD44<sup>+</sup>CD62L<sup>+</sup>); Tnaive, naïve T cell (CD44<sup>-</sup>CD62L<sup>-</sup>).

**NF- $\kappa$ B Response Assay.** The development of the CTL2-2 reporter cell line is described elsewhere (66). The experimental details are provided in *SI Appendix*.

**Quantitative Biodistribution Studies.** Quantitative biodistribution experiments were carried out as described previously (44). The experimental details are provided in *SI Appendix*.

**Ex Vivo Detection of Fluorescently Labeled Immunocytokines.** For fluorescent labeling, the proteins were resuspended in a 0.1 M sodium carbonate buffer at pH 9.1, and an excess of fluorescein isothiocyanate (FITC) was added. The reaction was carried out overnight at 4 °C. The labeled proteins were separated from unconjugated FITC by PD-10. Approximately 100  $\mu$ g of fluorescently labeled protein was injected into the lateral tail vein of tumor-bearing mice. The mice were euthanized 24 h after the injection. The organs were excised and embedded in NEG-50 cryoembedding medium (Thermo Fisher, Richard-Allan Scientific, 6502) before freezing. For staining, 8- $\mu$ m cryosections were fixed in acetone and incubated with goat anti-mouse CD31 (R&D Systems, AF3628, 1:200) and rabbit anti-FITC (Bio-Rad, 4510-7804), followed by donkey anti-goat AF594 (Invitrogen, A11058) and donkey anti-rabbit AF488 (Invitrogen, A21206). Images were acquired with a Zeiss AxioScope 2 Mot Plus fluorescence microscope with an Axiocam 503 camera at 200 $\times$  magnification in the RGB mode. The images were processed using ImageJ version 1.52k, with the thresholds set to 14 to 80 for the red channel and 15 to 100 for the green channel.

**Therapy Studies in s.c. Tumor Models.** After the s.c. implantation of the tumor cells into the right flank of the 8-wk-old female mice, tumor size was monitored by caliper measurements on a daily basis [volume = length  $\times$  width  $\times$  width  $\times$  0.5]. In the preventive setting, therapy was started when the tumor reached a volume of 40 mm<sup>3</sup>, and for the therapeutic setting, therapy was started when the tumors reached a volume of 75 to 100 mm<sup>3</sup>. The mice were grouped to obtain groups of similar average tumor size ( $n = 5$  or 6). The mice received 100  $\mu$ L of PBS (Gibco, 1010023), 500  $\mu$ g of F8(scFv)-4-1BBL, 200  $\mu$ g of  $\alpha$ PD-1 (Bio X Cell, clone 29F.1A12), or a combination of the checkpoint inhibitor and the immunocytokine. For the combination treatment, the checkpoint inhibitor was administered 1 d before the immunocytokine. The therapeutic agents were administered i.v. every second day in a total of three

cycles into the lateral tail vein. The animals were euthanized when the tumor diameter exceeded 15 mm or when the tumor began to ulcerate. Some cured mice were rechallenged by s.c. injection of WEHI-164 or CT26 tumor cells after being tumor-free for at least 4 wk. Statistical evaluations were done by standard two-way ANOVA followed by Tukey's multiple comparison test using GraphPad Prism 8.4.1.

**MRI and Glioblastoma Studies.** Coronal T2-weighted MRI images were acquired at day 12 after tumor implantation using ParaVision 6.0 software on a PharmaScan 4.7-T small animal magnetic resonance imager (Bruker Bio-Spin). The mean tumor perimeter at the maximum circumference was determined using Medical Image Processing, Analysis, and Visualization (MIPAV) software (<https://mipav.cit.nih.gov/>). Mice were euthanized when they manifested neurologic symptoms. Kaplan–Meier survival analysis was performed to assess survival differences among the treatment groups, and  $P$  values were calculated with the Gehan–Breslow–Wilcoxon test using GraphPad Prism 7.0a. Significance was tested at  $*P < 0.05$  and  $**P < 0.01$ .

**Analysis of Tumor-Infiltrating Lymphocytes by Flow Cytometry.** The mice were euthanized at 48 h after the second therapy cycle, and the tumor-draining lymph nodes as well as the tumor were excised. Detailed descriptions of the staining and analysis of the lymphocytes are provided in *SI Appendix*.

**Data Availability.** DNA sequences have been deposited in the GenBank database (accession nos. MW086510, MW086511, MW086512, MW086513, MW086514, MW086515, MW086516, MW086517, MW086518, MW086519, and MW086520). All study data are included in the main text and *SI Appendix*.

**ACKNOWLEDGMENTS.** We gratefully acknowledge the support of the Scientific Center for Optical and Electron Microscopy (ScopeM) of ETH Zurich. We thank Sabrina Müller and Fiona Amman for technical assistance, especially with protein production, and Lisa Nadal for help with some immunofluorescence staining. Financial support was provided by ETH Zürich, the Swiss National Science Foundation (310030\_182003/1), and the European Research Council under the European Union's Horizon 2020 research and innovation program (670603).

1. S. Lee, K. Margolin, Cytokines in cancer immunotherapy. *Cancers (Basel)* **3**, 3856–3893 (2011).
2. P. Murer, D. Neri, Antibody-cytokine fusion proteins: A novel class of biopharmaceuticals for the therapy of cancer and of chronic inflammation. *N. Biotechnol.* **52**, 42–53 (2019).
3. G. Dranoff, Cytokines in cancer pathogenesis and cancer therapy. *Nat. Rev. Cancer* **4**, 11–22 (2004).
4. G. Parmiani, L. Rivoltini, G. Andreola, M. Carrabba, Cytokines in cancer therapy. *Immunol. Lett.* **74**, 41–44 (2000).
5. R. Zappasodi, T. Merghoub, J. D. Wolchok, Emerging concepts for immune checkpoint blockade-based combination therapies. *Cancer Cell* **34**, 690 (2018).
6. C. Huttmacher, N. Gonzalo Núñez, A. R. Liuzzi, B. Becher, D. Neri, Targeted delivery of IL2 to the tumor stroma potentiates the action of immune checkpoint inhibitors by preferential activation of NK and CD8<sup>+</sup> T cells. *Cancer Immunol. Res.* **7**, 572–583 (2019).
7. E. Vacchelli et al., Trial Watch: Immunostimulation with cytokines in cancer therapy. *Oncolimmunology* **5**, e1115942 (2015).
8. S. A. Rosenberg, IL-2: The first effective immunotherapy for human cancer. *J. Immunol.* **192**, 5451–5458 (2014).
9. M. B. Atkins et al., High-dose recombinant interleukin 2 therapy for patients with metastatic melanoma: Analysis of 270 patients treated between 1985 and 1993. *J. Clin. Oncol.* **17**, 2105–2116 (1999).
10. V. R. Adams, T. Brenner, Oprelvekin (Neumega), first platelet growth factor for thrombocytopenia. *J. Am. Pharm. Assoc. (Wash)* **39**, 706–707 (1999).
11. M. I. Wilde, D. Faulds, Oprelvekin: A review of its pharmacology and therapeutic potential in chemotherapy-induced thrombocytopenia. *BioDrugs* **10**, 159–171 (1998).
12. P. B. Chapman et al., Clinical pharmacology of recombinant human tumor necrosis factor in patients with advanced cancer. *J. Clin. Oncol.* **5**, 1942–1951 (1987).
13. T. Taguchi, Clinical studies of recombinant interferon alfa-2a (Roferon-A) in cancer patients. *Cancer* **57**(suppl.8), 1705–1708 (1986).
14. R. J. Spiegel, INTRON A (interferon alfa-2b): Clinical overview. *Semin Oncol.* **13**, 89–101 (1986).
15. V. Limmroth, N. Putzki, N. J. Kachuck, The interferon beta therapies for treatment of relapsing-remitting multiple sclerosis: Are they equally efficacious? A comparative review of open-label studies evaluating the efficacy, safety, or dosing of different interferon beta formulations alone or in combination. *Ther. Adv. Neurol. Disord.* **4**, 281–296 (2011).
16. C. Madsen, The innovative development in interferon beta treatments of relapsing-remitting multiple sclerosis. *Brain Behav.* **7**, e00696 (2017).
17. C. H. Miller, S. G. Maher, H. A. Young, Clinical use of interferon-gamma. *Ann. N. Y. Acad. Sci.* **1182**, 69–79 (2009).
18. A. C. Herman, T. C. Boone, H. S. Lu, Characterization, formulation, and stability of Neupogen (Filgrastim), a recombinant human granulocyte-colony stimulating factor. *Pharm. Biotechnol.* **9**, 303–328 (1996).
19. J. Geigert, F. D. Ghrist, Development and shelf-life determination of recombinant human granulocyte-macrophage colony-stimulating factor (Leukine, GM-CSF). *Pharm. Biotechnol.* **9**, 329–342 (1996).
20. E. Vazquez, Leukine studies move forward. *Posit. Aware* **10**, 29 (1999).
21. F. Lejeune et al., Administration of high-dose tumor necrosis factor alpha by isolation perfusion of the limbs: Rationale and results. *J. Infus. Chemother.* **5**, 73–81 (1995).
22. J. P. Leonard et al., Effects of single-dose interleukin-12 exposure on interleukin-12-associated toxicity and interferon-gamma production. *Blood* **90**, 2541–2548 (1997).
23. P. F. Geertsens, M. E. Gore, S. Negrier, J. M. Tourani, H. von der Maase, Safety and efficacy of subcutaneous and continuous intravenous infusion rIL-2 in patients with metastatic renal cell carcinoma. *Br. J. Cancer* **90**, 1156–1162 (2004).
24. B. A. Baldo, Side effects of cytokines approved for therapy. *Drug Saf.* **37**, 921–943 (2014).
25. J. F. Eliason, Pegylated cytokines: Potential application in immunotherapy of cancer. *BioDrugs* **15**, 705–711 (2001).
26. J. A. Jazayeri, G. J. Carroll, Fc-based cytokines: Prospects for engineering superior therapeutics. *BioDrugs* **22**, 11–26 (2008).
27. D. H. Charych et al., NKTR-214, an engineered cytokine with biased IL2 receptor binding, increased tumor exposure, and marked efficacy in mouse tumor models. *Clin. Cancer Res.* **22**, 680–690 (2016).
28. E. T. Harvill, S. L. Morrison, An IgG3-IL2 fusion protein activates complement, binds Fc gamma RI, generates LAK activity and shows enhanced binding to the high-affinity IL-2R. *Immunotechnology* **1**, 95–105 (1995).
29. H. N. Lode, R. Xiang, J. C. Becker, S. D. Gillies, R. A. Reisfeld, Immunocytokines: A promising approach to cancer immunotherapy. *Pharmacol. Ther.* **80**, 277–292 (1998).
30. P. Hu et al., A chimeric Lym-1/interleukin 2 fusion protein for increasing tumor vascular permeability and enhancing antibody uptake. *Cancer Res.* **56**, 4998–5004 (1996).
31. J. Sharifi, L. A. Khawli, P. Hu, J. Li, A. L. Epstein, Generation of human interferon gamma and tumor necrosis factor alpha chimeric TNF-3 fusion proteins. *Hybrid. Biomedicines* **21**, 421–432 (2002).
32. M. L. Penichet, S. L. Morrison, Antibody-cytokine fusion proteins for the therapy of cancer. *J. Immunol. Methods* **248**, 91–101 (2001).
33. P. A. Young, S. L. Morrison, J. M. Timmerman, Antibody-cytokine fusion proteins for treatment of cancer: Engineering cytokines for improved efficacy and safety. *Semin. Oncol.* **41**, 623–636 (2014).
34. C. Halin et al., Enhancement of the antitumor activity of interleukin-12 by targeted delivery to neovasculature. *Nat. Biotechnol.* **20**, 264–269 (2002).
35. M. G. Lechner, S. M. Russell, R. S. Bass, A. L. Epstein, Chemokines, costimulatory molecules and fusion proteins for the immunotherapy of solid tumors. *Immunotherapy* **3**, 1317–1340 (2011).
36. P. M. Sondel, S. D. Gillies, Current and potential uses of immunocytokines as cancer immunotherapy. *Antibodies (Basel)* **1**, 149–171 (2012).



37. R. E. Kontermann, Antibody-cytokine fusion proteins. *Arch. Biochem. Biophys.* **526**, 194–205 (2012).
38. G. Fyfe *et al.*, Results of treatment of 255 patients with metastatic renal cell carcinoma who received high-dose recombinant interleukin-2 therapy. *J. Clin. Oncol.* **13**, 688–696 (1995).
39. M. Johannsen *et al.*, The tumour-targeting human L19-IL2 immunocytokine: Pre-clinical safety studies, phase I clinical trial in patients with solid tumours and expansion into patients with advanced renal cell carcinoma. *Eur. J. Cancer* **46**, 2926–2935 (2010).
40. T. K. Eigentler *et al.*, A dose-escalation and signal-generating study of the immunocytokine L19-IL2 in combination with dacarbazine for the therapy of patients with metastatic melanoma. *Clin. Cancer Res.* **17**, 7732–7742 (2011).
41. G. Spitaleri *et al.*, Phase III study of the tumour-targeting human monoclonal antibody-cytokine fusion protein L19-TNF in patients with advanced solid tumours. *J. Cancer Res. Clin. Oncol.* **139**, 447–455 (2013).
42. J. Strauss *et al.*, First-in-human phase I trial of a tumor-targeted cytokine (NHS-IL12) in subjects with metastatic solid tumors. *Clin. Cancer Res.* **25**, 99–109 (2019).
43. E. Puca, R. De Luca, F. Seehusen, J. M. M. Rodriguez, D. Neri, Comparative evaluation of bolus and fractionated administration modalities for two antibody-cytokine fusions in immunocompetent tumor-bearing mice. *J. Control. Release* **317**, 282–290 (2020).
44. A. Villa *et al.*, A high-affinity human monoclonal antibody specific to the alternatively spliced EDA domain of fibronectin efficiently targets tumor neo-vasculature in vivo. *Int. J. Cancer* **122**, 2405–2413 (2008).
45. J. N. Rybak, C. Roesli, M. Kaspar, A. Villa, D. Neri, The extra-domain A of fibronectin is a vascular marker of solid tumors and metastases. *Cancer Res.* **67**, 10948–10957 (2007).
46. E. S. White, F. E. Baralle, A. F. Muro, New insights into form and function of fibronectin splice variants. *J. Pathol.* **216**, 1–14 (2008).
47. K. Schwager *et al.*, A comparative immunofluorescence analysis of three clinical-stage antibodies in head and neck cancer. *Head Neck Oncol.* **3**, 25 (2011).
48. K. Schwager *et al.*, Preclinical characterization of DEKAVIL (F8-IL10), a novel clinical-stage immunocytokine which inhibits the progression of collagen-induced arthritis. *Arthritis Res. Ther.* **11**, R142 (2009).
49. R. G. Goodwin *et al.*, Molecular cloning of a ligand for the inducible T cell gene 4-1BB: A member of an emerging family of cytokines with homology to tumor necrosis factor. *Eur. J. Immunol.* **23**, 2631–2641 (1993).
50. K. E. Pollok *et al.*, 4-1BB T-cell antigen binds to mature B cells and macrophages, and costimulates anti-mu-primed splenic B cells. *Eur. J. Immunol.* **24**, 367–374 (1994).
51. M. A. DeBenedette *et al.*, Analysis of 4-1BB ligand (4-1BBL)-deficient mice and of mice lacking both 4-1BBL and CD28 reveals a role for 4-1BBL in skin allograft rejection and in the cytotoxic T cell response to influenza virus. *J. Immunol.* **163**, 4833–4841 (1999).
52. K. E. Pollok *et al.*, Inducible T cell antigen 4-1BB: Analysis of expression and function. *J. Immunol.* **150**, 771–781 (1993).
53. I. Melero, J. V. Johnston, W. W. Shufford, R. S. Mittler, L. Chen, NK1.1 cells express 4-1BB (CDw137) costimulatory molecule and are required for tumor immunity elicited by anti-4-1BB monoclonal antibodies. *Cell. Immunol.* **190**, 167–172 (1998).
54. R. S. McHugh *et al.*, CD4(+)/CD25(+) immunoregulatory T cells: Gene expression analysis reveals a functional role for the glucocorticoid-induced TNF receptor. *Immunity* **16**, 311–323 (2002).
55. A. Makkouk, C. Chester, H. E. Kohrt, Rationale for anti-CD137 cancer immunotherapy. *Eur. J. Cancer* **54**, 112–119 (2016).
56. A. V. Menk *et al.*, 4-1BB costimulation induces T cell mitochondrial function and biogenesis enabling cancer immunotherapeutic responses. *J. Exp. Med.* **215**, 1091–1100 (2018).
57. A. Bitra, T. Doukov, M. Croft, D. M. Zajonc, Crystal structures of the human 4-1BB receptor bound to its ligand 4-1BBL reveal covalent receptor dimerization as a potential signaling amplifier. *J. Biol. Chem.* **293**, 9958–9969 (2018).
58. A. Bitra *et al.*, Crystal structure of murine 4-1BB and its interaction with 4-1BBL support a role for galectin-9 in 4-1BB signaling. *J. Biol. Chem.* **293**, 1317–1329 (2018).
59. A. Bitra, T. Doukov, G. Destito, M. Croft, D. M. Zajonc, Crystal structure of the m4-1BB/4-1BBL complex reveals an unusual dimeric ligand that undergoes structural changes upon 4-1BB receptor binding. *J. Biol. Chem.* **294**, 1831–1845 (2019).
60. S. Fellermeier *et al.*, Advancing targeted co-stimulation with antibody-fusion proteins by introducing TNF superfamily members in a single-chain format. *Oncolimmunology* **5**, e1238540 (2016).
61. J. S. Huston *et al.*, Protein engineering of antibody binding sites: Recovery of specific activity in an anti-digoxin single-chain Fv analogue produced in *Escherichia coli*. *Proc. Natl. Acad. Sci. U.S.A.* **85**, 5879–5883 (1988).
62. R. E. Bird *et al.*, Single-chain antigen-binding proteins. *Science* **242**, 423–426 (1988).
63. P. Holliger, T. Prospero, G. Winter, “Diabodies”: Small bivalent and bispecific antibody fragments. *Proc. Natl. Acad. Sci. U.S.A.* **90**, 6444–6448 (1993).
64. C. Huttmacher, D. Neri, Antibody-cytokine fusion proteins: Biopharmaceuticals with immunomodulatory properties for cancer therapy. *Adv. Drug Deliv. Rev.* **141**, 67–91 (2018).
65. F. Bootz, D. Neri, Immunocytokines: A novel class of products for the treatment of chronic inflammation and autoimmune conditions. *Drug Discov. Today* **21**, 180–189 (2016).
66. J. Mock, C. Pellegrino, D. Neri, A universal reporter cell line for bioactivity evaluation of engineered cytokine products. *Sci. Rep.* **10**, 3234 (2020).
67. K. Frey, A. Zivanovic, K. Schwager, D. Neri, Antibody-based targeting of interferon- $\alpha$  to the tumor neovasculature: A critical evaluation. *Integr. Biol.* **3**, 468–478 (2011).
68. T. Hemmerle *et al.*, The antibody-based targeted delivery of TNF in combination with doxorubicin eradicates sarcomas in mice and confers protective immunity. *Br. J. Cancer* **109**, 1206–1213 (2013).
69. P. Probst *et al.*, Sarcoma eradication by doxorubicin and targeted TNF relies upon CD8<sup>+</sup> T-cell recognition of a retroviral antigen. *Cancer Res.* **77**, 3644–3654 (2017).
70. S. I. Mosely *et al.*, Rational selection of syngeneic preclinical tumor models for immunotherapeutic drug discovery. *Cancer Immunol. Res.* **5**, 29–41 (2017).
71. J. W. Yu *et al.*, Tumor-immune profiling of murine syngeneic tumor models as a framework to guide mechanistic studies and predict therapy response in distinct tumor microenvironments. *PLoS One* **13**, e0206223 (2018).
72. M. J. Selby *et al.*, Preclinical development of ipilimumab and nivolumab combination immunotherapy: Mouse tumor models, in vitro functional studies, and cynomolgus macaque toxicology. *PLoS One* **11**, e0161779 (2016).
73. A. Y. Huang *et al.*, The immunodominant major histocompatibility complex class I-restricted antigen of a murine colon tumor derives from an endogenous retroviral gene product. *Proc. Natl. Acad. Sci. U.S.A.* **93**, 9730–9735 (1996).
74. E. Puca *et al.*, The antibody-based delivery of interleukin-12 to solid tumors boosts NK and CD8<sup>+</sup> T cell activity and synergizes with immune checkpoint inhibitors. *Int. J. Cancer* **146**, 2518–2530 (2020).
75. A. C. Scott *et al.*, TOX is a critical regulator of tumour-specific T cell differentiation. *Nature* **571**, 270–274 (2019).
76. F. P. Canale *et al.*, CD39 expression defines cell exhaustion in tumor-infiltrating CD8<sup>+</sup> T cells. *Cancer Res.* **78**, 115–128 (2018).
77. C. Chester, S. Ambulkar, H. E. Kohrt, 4-1BB agonism: Adding the accelerator to cancer immunotherapy. *Cancer Immunol. Immunother.* **65**, 1243–1248 (2016).
78. J. Dubrot *et al.*, Treatment with anti-CD137 mAbs causes intense accumulations of liver T cells without selective antitumor immunotherapeutic effects in this organ. *Cancer Immunol. Immunother.* **59**, 1223–1233 (2010).
79. T. Bartkowiak *et al.*, Activation of 4-1BB on liver myeloid cells triggers hepatitis via an interleukin-27-dependent pathway. *Clin. Cancer Res.* **24**, 1138–1151 (2018).
80. X. Qi *et al.*, Optimization of 4-1BB antibody for cancer immunotherapy by balancing agonistic strength with Fc $\gamma$ R affinity. *Nat. Commun.* **10**, 2141 (2019).
81. S. K. Ho *et al.*, Epitope and Fc-mediated cross-linking, but not high affinity, are critical for antitumor activity of CD137 agonist antibody with reduced liver toxicity. *Mol. Cancer Ther.* **19**, 1040–1051 (2020).
82. M. Compte *et al.*, A tumor-targeted trimeric 4-1BB-agonistic antibody induces potent anti-tumor immunity without systemic toxicity. *Nat. Commun.* **9**, 4809 (2018).
83. K. Mikkelsen *et al.*, Carcinoembryonic antigen (CEA)-specific 4-1BB-costimulation induced by CEA-targeted 4-1BB-agonistic trimeric antibodies. *Front. Immunol.* **10**, 1791 (2019).
84. C. Claus *et al.*, Tumor-targeted 4-1BB agonists for combination with T cell bispecific antibodies as off-the-shelf therapy. *Sci. Transl. Med.* **11**, eaav5989 (2019).
85. M. J. Hinner *et al.*, Tumor-localized costimulatory T-cell engagement by the 4-1BB/HER2 bispecific antibody-anticalin fusion PRS-343. *Clin. Cancer Res.* **25**, 5878–5889 (2019).
86. D. Neri, Antibody-cytokine fusions: Versatile products for the modulation of anti-cancer immunity. *Cancer Immunol. Res.* **7**, 348–354 (2019).
87. S. D. Gillies, A new platform for constructing antibody-cytokine fusion proteins (immunocytokines) with improved biological properties and adaptable cytokine activity. *Protein Eng. Des. Sel.* **26**, 561–569 (2013).
88. T. Wüest *et al.*, TNF-selectokine: A novel prodrug generated for tumor targeting and site-specific activation of tumor necrosis factor. *Oncogene* **21**, 4257–4265 (2002).
89. L. Huyghe *et al.*, Safe eradication of large established tumors using neovasculature-targeted tumor necrosis factor-based therapies. *EMBO Mol. Med.* **12**, e11223 (2020).
90. A. Cauwels *et al.*, A safe and highly efficient tumor-targeted type I interferon immunotherapy depends on the tumor microenvironment. *Oncolimmunology* **7**, e1398876 (2017).
91. S. L. Pogue *et al.*, Targeting attenuated interferon- $\alpha$  to myeloma cells with a CD38 antibody induces potent tumor regression with reduced off-target activity. *PLoS One* **11**, e0162472 (2016).
92. D. Venetz, D. Koovely, B. Weder, D. Neri, Targeted reconstitution of cytokine activity upon antigen binding using split cytokine antibody fusion proteins. *J. Biol. Chem.* **291**, 18139–18147 (2016).
93. J. L. Bodmer, P. Schneider, J. Tschopp, The molecular architecture of the TNF superfamily. *Trends Biochem. Sci.* **27**, 19–26 (2002).
94. A. F. Labrijn, M. L. Janmaat, J. M. Reichert, P. W. H. I. Parren, Bispecific antibodies: A mechanistic review of the pipeline. *Nat. Rev. Drug Discov.* **18**, 585–608 (2019).
95. E. Dahlén, N. Veitonmäki, P. Norlén, Bispecific antibodies in cancer immunotherapy. *Ther. Adv. Vaccines Immunother.* **6**, 3–17 (2018).
96. C. Reichen *et al.*, Abstract 3029: FAP-mediated tumor accumulation of a T-cell agonistic FAP/4-1BB DARPin drug candidate analyzed by SPECT/CT and quantitative biodistribution. *Cancer Res.* **78**, 3029 (2018).
97. K. Hurvov *et al.*, A novel fully synthetic dual targeted Nectin-4/4-1BB Bicycle (R) peptide induces tumor localized 4-1BB agonism. *J. Immunother. Cancer* **7** (2019).
98. J. Muller, A. Baeyens, M. L. Dustin, Tumor necrosis factor receptor superfamily in T cell priming and effector function. *Adv. Immunol.* **140**, 21–57 (2018).
99. J. Li, Q. Yin, H. Wu, Structural basis of signal transduction in the TNF receptor superfamily. *Adv. Immunol.* **119**, 135–153 (2013).
100. E. S. Vanamee, D. L. Faustman, Structural principles of tumor necrosis factor superfamily signaling. *Sci. Signal.* **11**, eaao4910 (2018).
101. T. Weiss *et al.*, NKG2D-Dependent antitumor effects of chemotherapy and radiotherapy against glioblastoma. *Clin. Cancer Res.* **24**, 882–895 (2018).
102. T. Weiss, M. Weller, M. Guckenberger, C. L. Sentman, P. Roth, NKG2D-based CAR T cells and radiotherapy exert synergistic efficacy in glioblastoma. *Cancer Res.* **78**, 1031–1043 (2018).
103. B. Carnemolla *et al.*, Enhancement of the antitumor properties of interleukin-2 by its targeted delivery to the tumor blood vessel extracellular matrix. *Blood* **99**, 1659–1665 (2002).
104. N. Pasche, S. Wulhfard, F. Pretto, E. Carugati, D. Neri, The antibody-based delivery of interleukin-12 to the tumor neovasculature eradicates murine models of cancer in combination with paclitaxel. *Clin. Cancer Res.* **18**, 4092–4103 (2012).